A Viscoelastic Anisotropic Hyperelastic Constitutive Model of the Human Cornea

Charles Whitford[1*], Natalia V. Movchan[2] and Ahmed Elsheikh[1,3]

1 School of Engineering, University of Liverpool, L69 3GH, UK

2 Department of Mathematical Sciences, University of Liverpool, L69 3BX, UK

3 National Institute for Health Research (NIHR) Biomedical Research Centre at Moorfields Eye Hos-pital NHS Foundation Trust and UCL Institute of Ophthalmology, EC1V 9EL, UK

** corresponding author (whitford@liv.ac.uk)*

Abstract

200 word limit for abstract - current word count of 200

A constitutive numerical model based on the continuum mechanics theory has been developed which represents interlamellar cohesion, regional variation of collagen fib-ril density, 3D anisotropy and both age-related viscoelastic and hyperelastic stiffening behaviour of the human cornea. Experimental data gathered from a number of previ-ous studies on 48 ex vivo human cornea (inflation and shear tests) enabled numerical model calibration. Wide angle X-ray scattering and electron microscopy provided mea-sured data which quantifies microstructural arrangements associated with stiffness. The present study suggests that stiffness parallel to the lamellae of the cornea approximately doubles with an increase in strain-rate from 0.5 to 5%/min, while the underlying stromal matrix provides a stiffness 2-3 orders of magnitude lower than the lamellae. The model has been simultaneously calibrated to within 5% error across 3 age groups ranging from 50-95 years, multiple strain-rates and multiple loading scenarios. Age and strain-rate dependent material coefficients allow finite element modelling for an individual patient with material stiffness approximated by their age under varying loading scenarios. This present study addresses a significant gap in numerical representation of the cornea and has great potential in both daily clinical practice for the planning and optimisation of

Deleted: from

Deleted: of

Deleted: -

Deleted: . W

Comment [A1]: How many?

Comment [A2]: Two?

corrective procedures and in pre-clinical optimisation of diagnostic procedures.

Introduction

The ocular vessel consists of the cornea, sclera and corneoscleral limbal junction. The vessel protects the internal contents of the eye and maintains the eye's general shape, which is necessary for clear vision. The transparent cornea, at the anterior segment of the eye, provides two-thirds of the eye's optical power (Fatt, 1978), and this contribution is primarily determined by the cornea's external topography, clarity and refractive index relative to the external environment.

The topography of the cornea is determined by the balanced state between the forces acting upon it and its mechanical stiff ness, which is defined by cornea's geometry and thickness, and the material stiff ness. The term balanced state is often referred to as the equilibrium state. However, equilibrium refers specifically to static behaviour and this term is no longer appropriate while describing this relationship in the context of viscoelastic be-haviour. This is due to the dynamic state of the system, including the forces acting within the material and mass inertia of the system where equilibrium state is only achieved as time tends to infinity and both internal forces and inertia tend to zero. While the geometry and thickness, and their contribution to overall mechanical stiffness, are easy to determine, the material stiff ness is much more difficult to quantify as it is dependent on the microstructure of the stroma; the main load carrying layer of the cornea. The stroma is composed of over 200 lamellae (Freegard, 1997; Oyster, 1999), each of which formed of a proteoglycan-rich matrix containing tightly packed and ordered collagen fibrils. The density and orientation of collagen fibrils in the stroma are the primary factors affecting the material stiffness, and hence the overall mechanical stiff ness of the cornea (Jue et al., 1991; Newton and Meek, 1998; Boote et al., 2003, 2009). Wide angle X-ray scattering (WAXS) has been extensively used to detail the 2D anisotropic arrangement of collagen fibrils in the human cornea (Aghamoham-madzadeh et al., 2004; Meek and Boote, 2004; Boote et al., 2006). Further, the 3D organization of fibrils was observed by Komai and Ushiki (1991) using electron microscopy where the arrangement of lamellae and inter-lamellae fibrils was observed. Whitford et al. (2015) analysed the data within these studies and extracted relationships defining the regional variation of collagen fibril density and anisotropy across corneal surface.

To date there have been a significant number of studies which have progressed the numerical representation of the cornea in its quasi-static state. These have included

Deleted: al-

Deleted: and the sclera

Deleted: provides

Deleted: can be described in its simplest terms as the two intersecting spheres of the cornea and sclera

Deleted: . T

Deleted: to optical power

Deleted: its

Deleted: stress-free form

Comment [A3]: I am not sure this is needed

Deleted: The mechanical stiff ness of the cornea depends on its thickness and topography and

Deleted: , which is defined by

Deleted: :

Deleted: stroma

Deleted: formed

Deleted: from

Deleted: are

Deleted: arrangement

Deleted: and density

Deleted: contributors

Deleted: to

Deleted: bio

Deleted: has detailed the 2D anisotropic arrangement of collagen in the human cornea

Deleted: explored

Deleted: further

Deleted: The 3D organization of fibrils was observed by Komai and Ushiki (1991) using electron microscopy where the arrangement of lamellae and inter-lamellae fibrils was observed. Greater detail on the specific arrangement of fibrils is summarised in Whitford et al. (2015).

Alastrue et al. (2006); Pandolfi and Manganiello (2006); Pandolfi and Holzapfel (2008); Pinsky et al. (2005); Petsche and Pinsky (2013); Studer et al. (2010); Grytz and Meschke (2009, 2010); Nguyen and Boyce (2011); Whitford et al. (2015). Further, dynamic (non-static) behaviour of the cornea has been modelled in various studies. Glass et al. (2008) developed an isotropic, homogeneous, analytical model describing the effect of viscosity and elasticity on hysteresis in the human cornea. Perez et al. (2013) developed a viscoelastic model of the eye that was limited to linear-elastic, isotropic representation of porcine eyes with a homogeneous corneal representation. Kling et al. (2014) considered an isotropic, linear, viscoelastic corneal model within a multi-physics simulation of air-puff tonometry. Su et al. (2015) ?. Boyce et al. (2007) and Nguyen et al. (2008) developed viscoelastic constitutive models which were used to describe the behaviour of bovine cornea based on the results of strip-extensiometry.

To the author's knowledge, this is the first study that combines the com-plex anisotropic representation, shear stiffness and regional variation of fibril density of the human cornea with its viscoelastic behaviour. The study further attempts to calibrate the proposed model with existing ex vivo human data. The research builds on a recent study by the authors (Whitford et al., 2015) that introduced the representation of regional vari-ation of collagen fibril density and proposes a constitutive model that decomposes the stress-strain behaviour into four components representing (1) dilation, (2) isotropic matrix distortion response to both tension and compression, (3) anisotropic and regional variation of collagen fibrils, and (4) the time-dependent constituent which represents the non-linear, strain rate-dependence of behaviour

- **Deleted:** D
- **Deleted:** -
- **Deleted:** -
- **Deleted:** , however this model
- **Deleted:** context in
- **Deleted:** model
- **Deleted:** considering
- **Deleted:** h
- **Deleted:** , however those studies where limited to representation
- **Deleted:** there
- **Deleted:** are
- **Deleted:** no studies
- **Deleted:** which have
- **Deleted:** combined
- **Deleted:** either
- **Deleted:** know, and significant,
- **Deleted:** present
- **Deleted:** rectify this shortfall in knowledge and
- **Deleted:** s
- **Deleted:** In addition, the constitutive framework has the poten-tially be calibrated to appropriate in vivo experimental data as it becomes available.
- **Deleted:** A
- **Deleted:** the
- **Deleted:** . This previous model is included, and expanded upon, within the present study. The proposed
- **Deleted:** contributions
- **Deleted:** motivated by the micromechanics of the stroma: (1) to (3) representing the equilibrium response of the network and (4) a
- **Deleted:** of the network
- **Deleted:** relaxing and stiffening of the colla-gen fibrils with time as a
- **Deleted:** dependent
- **Deleted:** departure from the equilibrium
- **Deleted:**
- **Deleted:**

... [1]

Methods and Materials

Constitutive model

The non-linear anisotropic incompressible material behaviour of the corneal stroma can be numerically represented using a strain-energy density function:

$$\psi = \psi\,[C, A, B]\,, \tag{1}$$

where C is the right Cauchy-Green deformation tensor calculated from the deformation gradient. $C = F^T F$ with F being a second order tensor representing the gradient of the mapping function which relates the current configuration of a continuum to its reference configuration. $A = a \otimes a$ and $B = b \otimes b$ are anisotropic tensors, based on vectors a and b which define single discretised directions of anisotropy. Similar to a procedure presented earlier (Studer et al., 2010), an isochoric split is performed on the energy density function to separate the responses to a volume-changing dilation and a volume-preserving distortion:

$$\psi = U\,[J] + \bar{\psi}\left(\bar{C}, A, B\right), \tag{2}$$

where $\bar{C}$ is the distortion component of the right Cauchy-Green deformation tensor defined from $\bar{C} = J^{2/3}$ I C = $J^{2/3}$ C where I represents the unit tensor, J = det F, $\bar{F} = J^{1/3}$ I F and $\bar{F}$ defines the deformation gradient associated with distortion. Further explanation of these concepts is provided by Holzapfel (2000) and others. In order to provide separate representations of the matrix' and fibrils' contributions to mechanical behaviour, a second split of the strain energy function is performed:

$$\psi = U\,[J] + \bar{\psi}_m\left(\bar{C}\right) + \bar{\psi}_f\left(\bar{C}, A, B\right), \tag{3}$$

4

Deleted: ... [2]

Deleted: , F as

Deleted: is

Deleted: a

As in Whitford et al. (2015) and other studies, the dilation constituent, U [J], from Eqn. 3 is given by:

$$U[J] = \frac{1}{D}(J-1)^2, \quad (4)$$

where D is the material coefficient describing volume change. Also in the neo-Hookean formulation, the constituent equation to represent the matrix stiffness is given by:

$$\bar{\psi}_m(\bar{I}_1) = C_{10}(\bar{I}_1 - 3), \quad (5)$$

where the distortion component of the right Cauchy-Green deformation tensor, $\bar{C}$, was replaced by its first strain invariant; $\bar{I}_1 = \mathrm{tr}\bar{C}$, and C_{10} is a material constant.
Since in this equation A and B are second order tensors and each can only represent a single direction of anisotropy, an adaptation is required to enable consideration of a multi-directional fibril orientation. Pinsky et al. (2005) presented a numerical method to describe the angular distribution of collagen fibrils in the corneal and limbal stroma obtained from WAXS studies (Aghamohammadzadeh et al., 2004). This method was later modified by Studer et al. (2010). The coordinate system adopted is presented in Whitford et al. (2015). Also from Whitford et al. (2015) the strain-energy function describing the fibril response is given by:

$$\psi_f(\bar{C}, A, B) = \zeta \frac{1}{\pi}\int_0^{\pi} \left(\psi_{f,lamellae} + \psi_{f,ILC}\right) d\theta_L, \quad (6)$$

The lamellae and ILC fibril contributions to the constituent equation were based on the polynomial Ogden law, modified by Markert et al. (2005) to include one direction of anisotropy. They were therefore rewritten as:

$$\psi_{f,lamellae}(\bar{I}_4) = \frac{\mu_1}{\gamma_1}\left(\bar{I}_4^{\frac{\gamma_1}{2}} - 1\right) - \mu_1 \ln \bar{I}_4^{\frac{1}{2}},$$
$$\psi_{f,ILC}(\bar{I}_6) = \frac{\mu_2}{\gamma_2}\left(\bar{I}_6^{\frac{\gamma_2}{2}} - 1\right) - \mu_2 \ln \bar{I}_6^{\frac{1}{2}}, \quad (7)$$

where $\bar{C}$, A and B in Eqn. 6 are replaced by the invariants $\bar{I}_4 = \bar{C} : (a \otimes a)$, $\bar{I}_6 = \bar{C} : (b \otimes b)$ and material parameters μ (polynomial coefficient relating to stiffness) and γ (governing nonlinearity relating to hyperelasticity).

The condition where the fibril constituent of Eqn. 3 is only activated where tension is applied, $\lambda_{4,6} = I_{4,6}^{\frac{1}{2}} > 1$, as it is considered that only the matrix carries compressive forces.

Numerical parameters ζ and χ represent the global and local distributions of collagen fibrils respectively. The derivation and definitions of these parameters can be found in Whitford et al. (2015).

To accommodate rate-dependency within the model the response of the material becomes a function of time, $t \in [0, T]$, where reference time $t = 0$ relates to the refer-ence configuration, Ω_0. Viscoelastic effects are described using the concept of internal variables. These variables are not accessible to direct observation; they describe the internal structure of the material associated Holzapfel et al. (2000). Viscoelastic behaviour is modelled by $m \geq 1$ relaxation processes with corresponding relaxation times,

$\tau_\alpha \in [0, \infty]$, $\alpha = 1, \cdots, m$ $(m \geq 1)$, describing the rate of decay of the stress. These material variables vanish at the equilibrium state; which does not depend on time. The internal variables are denoted by $_\alpha$, $\alpha = 1, \cdots, m$.

Mathematically, the adaptation of the model to represent viscoelastic response could be performed prior to the isochoric split, or the split between matrix and fibril def-initions, therefore accommodating viscoelastic behaviour of the dilation and/or the matrix within the model. However, the matrix and dilation contributions to stiffness have been shown to have relatively less contribution to stiffness than fibril behaviour (Whitford et al., 2015). Further, insufficient knowledge prohibits the inclusion of vis-coelastic representation of the matrix due to lack in experimental data with which to calibrate such a model. Holzapfel and Gasser (2001) presented a model where the viscoelastic behaviour was a function of the distortion component of the strain-energy after the isochoric split had been performed. That model is modified here and the dis-sipative potentials are introduced providing the viscoelastic constituent as a function of the fibril constituent, $\sum_{\alpha=1}^{m} \bar{\Upsilon}^{\infty}_{f\alpha}(\bar{C}, A, B, \bar{\Gamma}_\alpha)$. The 4^{th} and 6^{th} tangential and out-of-tangential fibril constituents of the model being functions of the 4^{th} and 6^{th} strain invariants respectively leads to $\sum_{\alpha=1}^{m} \sum_{a=4,6} \bar{\Psi}^{\infty}_{f\alpha a}(\bar{C}, \bar{I}_a, \bar{\Gamma}_\alpha)$, and the strain-energy function from

Comment [A4]: not clear

Comment [A5]: if this is true you will have problems calibrating your model in this paper

Eqn. 3 becomes:

$$\psi = U^{\infty}[J] + \psi_m\left(\bar{I}_1^{\infty}\right) + \psi_f\left(\bar{I}_{4,6}^{\infty}\right) + \sum_{\alpha=1}^{m} \Upsilon_{f\alpha}^{\infty}\left(\bar{C}, \bar{I}_{4,6}, \alpha\right) \tag{8}$$

At this stage the symmetric second Piola-Kirchhoff stress tensor can be written describing the equilibrium stress response of the material:

$$S^{\infty} = S_{dil}^{\infty} + S_m^{\infty} + S_f^{\infty}. \tag{9}$$

The three contributions to the constitutive model, S^{∞}_{dil}, S^{∞}_{m} and S^{∞}_{f}, describe the dilation, and the isotropic and anisotropic distortion responses of the matrix and fibres respectively. These are given by:

$$S_{dil}^{\infty} = 2\frac{\partial U^{\infty}}{\partial C}, \quad S_m^{\infty} = 2\frac{\partial \psi^{\infty}}{\partial C}, \quad S_f^{\infty} = 2\frac{\partial \psi_f^{\infty}}{\partial C} \tag{10}$$

From Holzapfel and Gasser (2001) the rate-dependency is expressed as an additional component to the constitutive equation at time t_{n+1} and an adaptation the stress function is required where the non-equilibrium stresses, $Q_\alpha = J^{-2/3}\,P : \hat{Q}_\alpha$ where the 4th order projection tensor, P, is given by:

$$P = I - C^{-1} \otimes (C/3), \quad I_{IJKL} = \left(\delta_{IK}\delta_{JL} + \delta_{IJ}\delta_{KL}\right)/2 \tag{11}$$

$$\hat{Q}_\alpha = 2\frac{\partial \psi_{f\alpha}\left(\bar{C}, A, B\right)}{\partial \bar{C}}. \tag{12}$$

The internal dissipation is defined as: $D_{int} = \sum_{\alpha=1}^{m} Q_\alpha : \dot{\Gamma}_\alpha/2 \geq 0$. As the dissipation vanishes at equilibrium ($t \to \infty$)

$$Q_\alpha = -2\frac{\partial \psi_{f\alpha}}{\partial \Gamma_\alpha}\Big|_{t\to\infty} = 0, \quad \alpha = 1, \cdots, m \tag{13}$$

and Eqn. 9 becomes:

$$S_{n+1} = \ldots \sum^{m} \ldots_{n+1} \tag{14}$$

Comment [A6]: unclear

where the non-equilibrium stresses are defined by:

$$(Q_\alpha)_{n+1} = (H_\alpha)_n + \beta_\alpha^\infty \exp(\xi_\alpha)\, S_f^\infty{}_{n+1}, \quad \alpha = 1, \cdots, m \tag{15}$$

and the definition of the history term, $(H_\alpha)_n$, $\alpha = 1, \cdots, m$, is modified from Holzapfel and Gasser (2001) providing

$$(H_\alpha)_n = \exp(\xi_\alpha)\left[\exp(\xi_\alpha)(Q_\alpha)_n - \beta_\alpha^\infty S_f^\infty{}_n\right], \quad \xi_\alpha = -\frac{t}{2\tau_\alpha} \tag{16}$$

$\beta_\alpha^\infty \in [0, \infty]$ and $\tau_\alpha \in [0, \infty]$, $\alpha = 1, \cdots, m$ are non-dimensional and time-dimensional strain-energy factors respectively. These remain to be defined. For mathematical pur-poses the potentially inaccurate approximation is made that the viscoelastic stress of the reference configuration, $Q_\alpha^{0+} = 0$. The accuracy of this approximation relates to the implementation of the constitutive model and is discussed later in the study. The stiff ness tensor at t_{n+1} can similarly be written as:

$$D_{n+1} = \left(D_{dil}^\infty + D_m^\infty + D_f^\infty + \sum_{\alpha=1}^{m} D_{vis}^\alpha\right)_{n+1} \tag{17}$$

where

$$D_{dil}^\infty = 2\frac{\partial S_{dil}^\infty}{\partial C}, \quad D_m^\infty = 2\frac{\partial S_m^\infty}{\partial C}, \quad D_f^\infty = 2\frac{\partial S_f^\infty}{\partial C} \tag{18}$$

and

$$(D_{vis}^\alpha)_{n+1} = \delta_\alpha\, D_f^\infty{}_{n+1}, \quad \delta_\alpha = \beta_\alpha^\infty \exp(\xi_\alpha), \quad \alpha = 1, \cdots, m \tag{19}$$

Implementation of numerical simulation

Numerical simulations have been conducted using finite element analysis (FEA). Geo-metric modelling was performed using bespoke software that provides geometry, which can be imported into finite element solvers as an orphan mesh. Finite element solver Abaqus/Standard 6.13 (Dassault Systmes Simulia Corp., Rhode Island, USA) was used. Abaqus is well known for its ability to analyse non-linear problems. However, its abil-ity to provide state-of-the-art representation of biological material properties, and both regional and local variation of these properties, is limited. Thus, Abaqus was used in conjunction with bespoke subroutines (SDVINI & UMAT) written in FORTRAN to implement the constitutive model described above.

The integral of Eqn. 6 was discretized into steps of one degree by $\frac{1}{\pi}\int_0^\pi d\theta_L \rightarrow \frac{1}{180}\sum_{i=1}^{180}\theta_{L,i}$, where $\theta_{L,i}$ defines the orientation of the one hundred and eighty directions of anisotropy per integration point within the model. The assumption that ~~all fibrils are straight is considered here, such that the range of the integral is only 1 − 180° and the condition where~~ the fibril constituent of the model only provided tensile stiffness was adopted throughout all behaviour stages.

Subroutine SDVINI was used to provide initial, reference-configuration and location-based conditions such as fibril density representation. These location-based properties are defined individually for each integration point.

These are implemented into the numerical simulation using the UMAT subroutine as demonstrated in the Abaqus User Subroutines Reference Guide (?). UMAT is also used to define current-configuration properties such as anisotropy.

Models were generated using fifteen-noded, solid, hybrid, quadratic elements (Abaqus, C3D15H). Elements were arranged in three layers and in twenty six rings. The shape of elements, and their arrangement, was chosen to provide uniform element sizes and consistent approximation of geometry. The near-incompressibility of the corneal stroma is represented by hybrid elements which provide volume controls within the solver (Abaqus Theory Manual), and the constant D (Eqn. 4) was set to the low value of 10^{-5}, indicating close to incompressible behaviour. Similar to Pandolfi and Holzapfel (2008): the remaining dilation term of Eqn. 8 becomes purely mathematically moti-vated. The arrangement of elements, three layers and twenty four rings, (Figure 1) was chosen by increasing the number of element layers and rings by assessing the conver-gence of the solution. The number of element rings was controlled by the number of element layers such that the aspect ratio of the elements approached 1. The number of layers, and therefore rings, was increased until the difference of apical deformation in the subsequent simulation with further refinement became less than 0.1%. C3D15H elements contain nine integration points. It was judged that the number of elements

Formatted: Strikethrough

Comment [A7]: I would not use this statement as reviewers may argue that fibrils are not straight, at least under low stresses -

Deleted: applied for each element in each discretized direction of anisotropy

Deleted: ,

Deleted: n

provided good refinement regarding the regional variation of material properties, which were individually characterised for each integration point.

Derivation of material properties

(a)

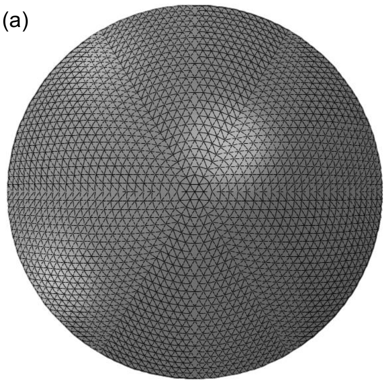

(b)

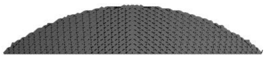

Figure 1: Finite element model (FEM) of the human cornea: (a) anterior view; (b) side elevation view

Deleted: section

Characteristic experimental data has been obtained from 48 fresh human donor corneas. Data includes 36 corneas tested under inflation and 12 corneas tested under shear. The corneas tested under inflation were divided into two groups: 23 corneas tested with 37.5 mmHg/min pressure rate and 13 corneas tested with 3.75 mmHg/min rate (Elsheikh et al., 2007). The age range of the two groups was 51 − 95 (77.6 ± 13.2) and 50 − 95 (75.7 ± 14.2) years, respectively. Within each group, the corneas were divided into three age subgroups: 50 − 64, 65 − 79, and 80 − 95 years. The number of corneas tested under 37.5 mmHg/min was 4, 6, and 13 within the three age subgroups, respectively. The corresponding numbers tested under 3.75 mmHg/min were 4, 4, and 5. 12 human donor corneas, aged between 61 and 74 years (67.7 ± 5.8), were tested to determine the behaviour of stromal tissue under surface shear at a shear deformation rate of 10%/min (with respect to the tissue's thickness) (Elsheikh et al., 2009). Shear tests do not generate strains parallel to the tangent plane; allowing the isolation of out-of-tangential behaviour during numerical analysis. In contrast, inflation generates multi-axis strain, including relatively large tangential strains. The isolation of material behaviour through multi-objective experimental fitting was utilised in Whitford et al. (2015) and is again utilised in this study. In addition to this isolation of anisotropic stiffness calibration the 3 different loading rates allow the simultaneous calibration of viscoelastic parameters.

Comment [A8]: Missing something

There are only 2 loading rates

Comment [A9]: unclear

The external parameters (ζ, χ) describing the local and global variation in fibril distribution and the internal parameters (C_{10}, D) which describe the stiffness of the matrix and the volume change are unaffected by the introduction of the internal variables which relate to the viscoelastic behaviour. These values therefore remain as derived in Whitford et al. (2015). However the internal parameters ($\mu_{1,2}$, $\gamma_{1,2}$) are intrinsically combined with the viscoelastic parameters in the partial differential equations of the viscoelastic behaviour. Further, in earlier studies describing the anisotropic distribu-tion of collagen fibrils, for example (Pinsky et al., 2005; Studer et al., 2010; Whitford et al., 2015), the material parameters were derived to define the hyperelastic response at a non-equilibrium state. The inclusion of the viscoelastic term in the fibril repre-sentation requires that parameters $\mu_{1,2}$, $\gamma_{1,2}$ describing the fibril response are redefined such that they are intended to represent the equilibrium behaviour. The parameters which remain to be determined ($\mu_{1,2}$, $\gamma_{1,2}$, β_α, τ_α : $\alpha = 1, \cdots, m$), were derived using a multi-objective inverse analysis procedure. This optimisation process used a combina-tion of bespoke software and the optimisation software HEEDS (Red Cedar Technology, Michigan, USA). Within HEEDS, the SHERPA algorithm was utilised. This algorithm incorporates Monte Carlo sampling; this ensured that the analysis did not stop at local minima and that the resulting values were unique and robust. The objectives were to reduce the root-mean square (RMS) errors between the characteristic experiment results for corneal shear and inflation and their respective numerical simulations. In the study by Whitford et al. (2015) the parameters defining shear behaviour could be derived independently as the parameters defining tangential stiffness had no influence on this behaviour. However, due to the necessary approximation that the viscoelastic

Deleted: to

Comment [A10]: cannot we only refer to Heeds. If you mention bespoke software, you will need to provide full details.

behaviour of the interlamellae fibrils is the same as the lamellae fibrils the viscoelastic parameters for both family of fibrils require simultaneous derivation. The constitutive model above has been expressed for multiple orders of viscoelastic behaviour which can be represented through the use of the α term ($\alpha = 1, \cdots, m$). The derivation process for material parameters included trials to determine the appropriate value for m.

Results

Numerical simulations were fitted to characteristic experimental data (Figure 2). Ini-tial trials were conducted utilising a first-order viscoelastic model during which a root-mean-square error (RMS) for the age group 80−95 years of 4% of the total deformation simulated (200 − 550 μm) was achieved. However, with decreasing age, the RMS in-creased to 5% for age group 50 − 65; the RMS for shear inflation was 3%. The fitting trend between age groups resulted in overestimation of displacement at low IOP and underestimation at higher IOP for the 50 − 65 age groups with a reversal of this trend when representing the 80 − 95 age-group. Inverse analysis trials to derive material pa-rameters were also conducted on a second-order viscoelastic model. For these separate trials the RMS for all age-groups and loading-rates of inflation simulations and shear was less than 3%. The greatest error (***%) was in the youngest age group.

Parameters of the proposed model have been simultaneously determined to represent characteristic shear and inflation responses across 3 different loading rates and for 3 age groups (Table 1 and Figure 3). As described above, during the multiple iterations of analysis both γ_2 and μ_2, governing the equilibrium behaviour of ILC fibrils, were free to optimise. However, the output of the procedures consistently provided values within 0.05% of each other. Due to this non-significant difference, results have been provided based on the mean of these values and are therefore constant with age. Parameters γ_1,

μ_1, β_1 and β_2 are non-dimensional, γ_1 decreases, and μ_1, β_1 and β_2 increase, with age. τ_1 and τ_2 have units of seconds and increase with age.

Stiffness varies directionally and by location across the entire cornea as previously described. Figure 4 provides the stiffness relationships at selected discrete locations

Deleted: lamellee

Deleted: lamellee

Comment [A11]: I would just say that the RMS remained below 5% for parameter optimisation in all age groups and in both inflation and shear tests

Comment [A12]: Is that necessary – what is important is that there is a close match and a low RMS

Deleted: for

Deleted: esent

Comment [A13]: 2

Deleted: previously

Comment [A14]: ?

Comment [A15]: Unclear – these are different parameters – how come their values were very close to each other?

Deleted: over

Comment [A16]: Shouldn't this go to methods section?

Comment [A17]: Why is that important?

Comment [A18]: Is this something known from before or a result of your study? If the latter, make it clear it is an outcome and show evidence.

Comment [A19]: Make it clear that tangent modulus is used as a measure of stiffness

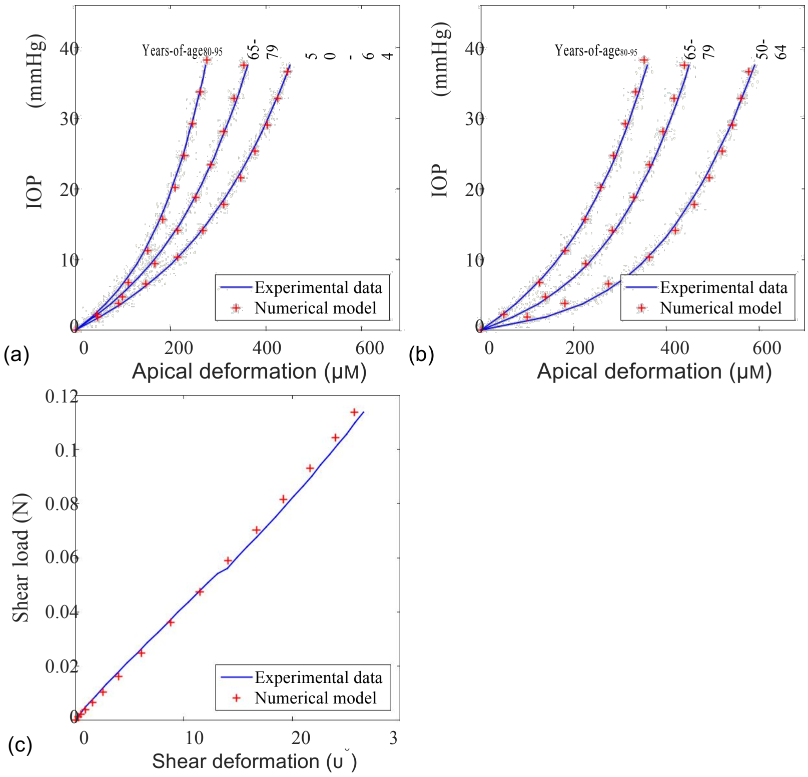

Figure 2: Characteristic experimental data and results of numerical simulation: (a) corneal inflation, 37.5 mmHg/min; (b) corneal inflation, 3.75 mmHg/min; (c) corneal shear, 10%/min deformation

Table 1: Numerical parameters derived for the constitutive model describing the anisotropic, viscoelastic and hyperelastic corneal behaviour from 50 to 95 years-of-age

Comment [A20]: You have considered different (3) age groups in text

Parameter	Value
D (-)	10^{-5}
C_{10} (-)	0.009
μ_2 (-)	3.85
γ_2 (-)	7.42×10^{-6}

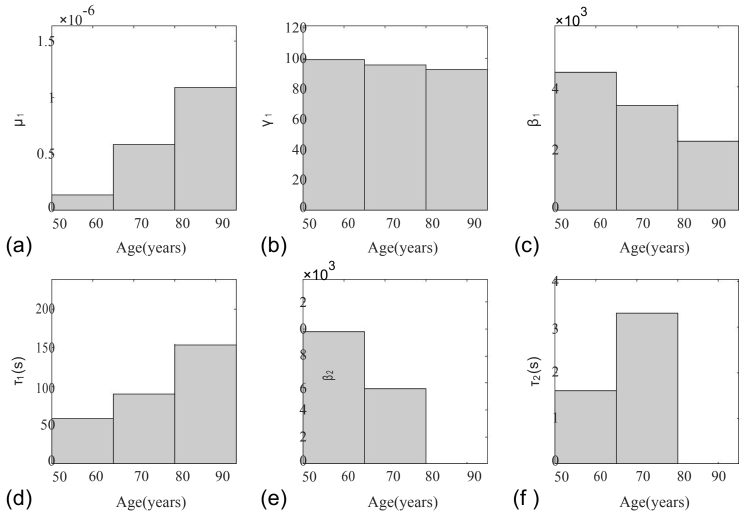

Figure 3: Numerical parameters (μ_1(a), γ_1(b), β_1(c), τ_1(d), β_2(e) and τ_2(f)) derived for the constitutive model describing the anisotropic, viscoelastic and hyperelastic corneal behaviour from 50 to 95 years-of-age. Bar chart provides the discrete values derived for the best fit with each age group. Other numerical parameters are constant with age and are presented in Table 1.

Comment [A21]: In some cases, values are zero – is that OK?

and directions across the cornea and varying strain rates. Figures 4a-c provide the hyperelastic stress-strain relationships on the tangential plane of the cornea at 0.5% and 5%/min strain. Consistently the higher strain-rate results in higher stiffness when compared to the same location and direction. The greatest stiffness is observed circum-ferentially at the limbus. Of the stiffness relationships presented, the lowest stiffness is in the diagonal direction at the corneal pole. Figure 4d provides the linear stress-strain relationship under shear at 10%/min, where this strain-rate relates to translational motion of the top surface of the cornea in relation to the lower surface with respect to its thickness. Figure 4e highlights the tangent modulus at 2% strain and Figure 4f presents the shear stiffness. From figures 4e & 4f it is clear that the shear stiffness is significantly less than tangential stiffness at 31.5 kPa compared to the range presented across the cornea for tangential stiffness, 370 − 1738 kPa. At the presented strain the strain-rate of 5%/min is almost double that at 0.5%/min for the respective location and direction.

Comment [A22]: Unclear – what is double? Do you mean stiffness?

Discussion

Within this study, a numerical representation of corneal microstucture has been developed within a continuum framework and applied to FEA. The model was applied to an extensive experimental database to obtain numerical relationships which describe regional variation of collagen density and anisotropy; the lamellae and ILC stiffness; the stiffness variation with age; strain-rate dependent viscoelastic behaviour; and the viscoelastic variation with age (density and anisotropy being described in earlier studies such as Whitford et al. (2015)). As in Whitford et al. (2015), density and anisotropic distribution of fibrils could not be observed or modelled with respect to age. It was suggested in that earlier study that variation in stiffness with age could be a function of fibril behaviour, not arrangement. This hypothesis is expanded and reinforced in the current study due to the ability of the model to accurately and simultaneously represent age-related stiffening and age-related viscoelasticity changes without the need to change mircostructural arrangement representation.

Deleted: the

Deleted: the

Comment [A23]: ?

Deleted: by

Deleted: this

Deleted: as the basis for this hypothesis is

Deleted: stiffness

Deleted: requirement

The results of the calibration of the new constitutive model which has been presented

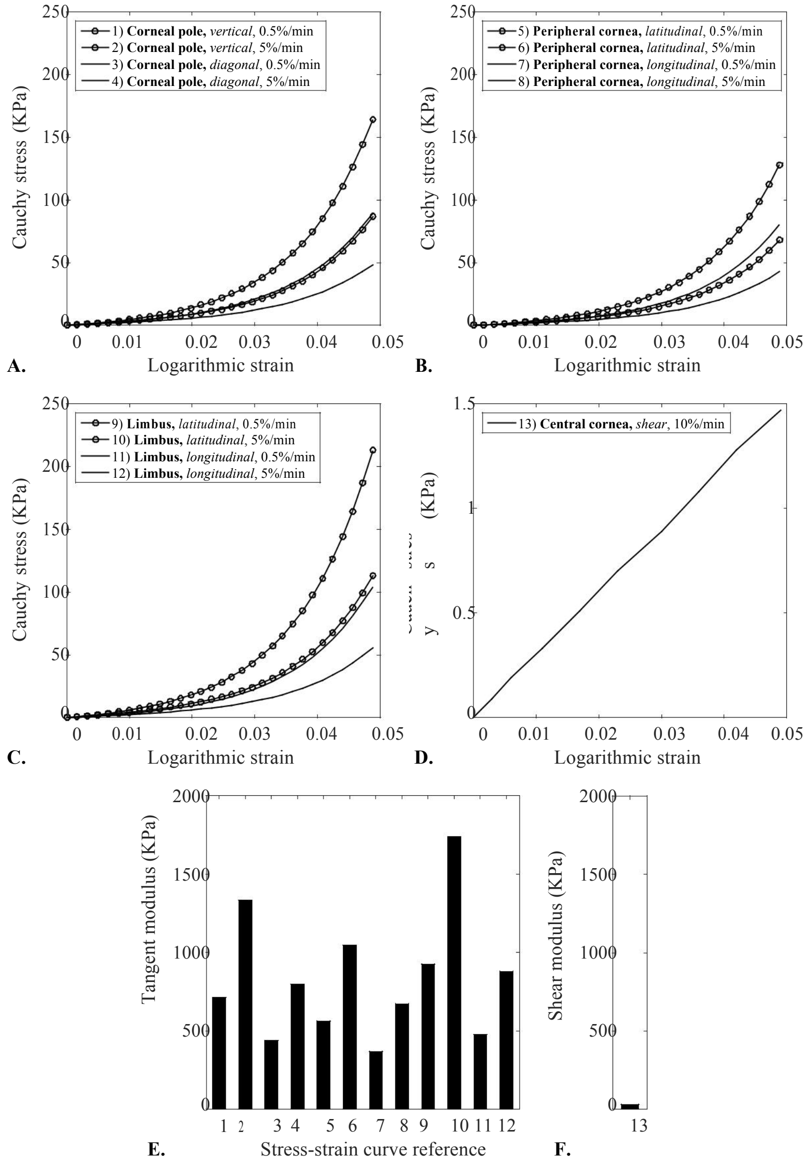

Figure 4: Material stiff ness relationships representing characteristic behaviour of a 87 year old: (a-c) regional and directional specific stress-strain behaviour obtained parallel to the tangent plane; (d) stress-strain relationship representing shear behaviour (note the diff erent scale on the stress axis compared with plots (a-c)); (e) tangent modulus for stress-strain relationships 1-12; (f) shear modulus. Values represent the stiff ness at 0.02 logarithmic strain.

Comment [A24]: Figure uses A, B and text uses a, b

Comment [A25]: What are 1 to 12?

Comment [A26]: I cannot see any variation in (F) here is the relationship between viscoelastic behaviour and age. Previous presentations of the cornea's strain-rate dependent stiffness have not been able to isolate the age-related stiffening from the age-related viscoelastic changes. In the new constitutive model, parameters defining the viscoelastic behaviour, β and τ, define the initial stage of non-equilibrium behaviour including the rate of decay of the non-equilibrium proportion. It has been shown that both the rate of decay and initial proportion increase with age. However, during trials it was found that a second contribution to viscoelasticity was required to provide a reasonable representation particularly in the youngest age-group, this contribution to viscoelasticity tended to zero in the age-group 80 − 95 years-of-age. Such a finding may be of increased importance where the application of high-speed techniques, such as non-contact tonometry, are utilised to determine ocular behaviour as this second contribution had a dissipation period of ≈ 2 seconds for 50 − 65 year olds.

The model which has been presented here introduces a viscoelastic constituent to the model presented by Whitford et al. (2015). That model attributed the regional and anisotropic distribution of stiffness to fibril density and arrangement. In this model the viscoelasticity decays with time ($t \to \infty$), with its initial contribution being pro-portional to the behaviour of the fibrils. This is a potentially inaccurate assumption as the viscoelastic behaviour could have contributions from the matrix components of the stroma. However, these components have been shown to have relatively low stiffness and therefore it is suggested that inaccuracies in this assumption would not lead to large inaccuracies in the overall behaviour of the model.

The intention, and potential capacity, of this constitutive model is that exclusion of the viscoelastic material component provides a model of the equilibrium state of the material. However, it is not possible to directly derive the equilibrium behaviour from the material parameters which have been presented here. This fact is due to the limita-tions of the fitting procedure which was limited to three loading rates (two inflation and one shear). The material parameters which have been presented are only valid within the strain-rates from which they were derived and direct derivation of the equilibrium would require extrapolation.

Deleted: -

Deleted: load

Deleted: based

Deleted: , equilibrium behaviour

Deleted: behaviour

Deleted: The adopted

Deleted:

Deleted: proportion

Comment [A27]: unclear

Comment [A28]: unclear

Deleted: , in this case, the equilibrium behaviour of the fibrils, and

Comment [A29]: what do you mean by proportion – is it stagte?

Comment [A30]: I think this is dangerous – reviewers can see it as a "fudge" parameter – I would not include this – you simply say this parameter tended to zero in certain age groups.

Conclusions

Comment [A31]: Usually there is not a conclusions section, but a final paragraph explaining main findings and their significance.

!!! Conclusion will be written once journal is selected and the main document has been finalised. !!!

Bibliography

Aghamohammadzadeh, H., Newton, R. H., Meek, K. M., feb 2004. X-ray scattering used to map the preferred collagen orientation in the human cornea and limbus. Structure 12 (2), 249–56.
URL http://www.ncbi.nlm.nih.gov/pubmed/14962385

Alastrue, V., Calvo, B., Pena, E., Doblare, M., 2006. Biomechanical Modeling of Refractive Corneal Surgery. Journal of Biomechanical Engineering 128 (1), 150.
URL http://link.aip.org/link/JBENDY/v128/i1/p150/s1{&}Agg=doi

Boote, C., Dennis, S., Newton, R. H., Puri, H., Meek, K. M., jul 2003. Collagen fibrils appear more closely packed in the prepupillary cornea: optical and biomechanical implications. Investigative Ophthalmology & Visual Science 44 (7), 2941–8.
URL http://www.iovs.org/cgi/doi/10.1167/iovs.03-0131

Boote, C., Hayes, S., Abahussin, M., Meek, K. M., mar 2006. Mapping collagen organi-zation in the human cornea: left and right eyes are structurally distinct. Investigative Ophthalmology & Visual Science 47 (3), 901–908.
URL http://www.ncbi.nlm.nih.gov/pubmed/16505022

Boote, C., Hayes, S., Young, R. D., Kamma-Lorger, C. S., Hocking, P. M., Elsheikh, A., Inglehearn, C. F., Ali, M., Meek, K. M., may 2009. Ultrastructural changes in the retinopathy, globe enlarged (rge) chick cornea. Journal of Structural Biology 166 (2), 195–204.
URL http://www.pubmedcentral.nih.gov/articlerender.fcgi?artid=2680986{&}tool=pmcentr

Boyce, B. L., Jones, R. E., Nguyen, T. D., Grazier, J. M., jan 2007. Stress-controlled

viscoelastic tensile response of bovine cornea. Journal of Biomechanics 40 (11), 2367– 76.
URL http://www.ncbi.nlm.nih.gov/pubmed/17240381

Elsheikh, A., Ross, S., Alhasso, D., Rama, P., jan 2009. Numerical study of the eff ect of corneal layered structure on ocular biomechanics. Current Eye Research 34 (1), 26–35.
URL http://www.ncbi.nlm.nih.gov/pubmed/19172467

Elsheikh, A., Wang, D., Brown, M., Rama, P., Campanelli, M., Pye, D., jan 2007. Assessment of corneal biomechanical properties and their variation with age. Current Eye Research 32 (1), 11–19.
URL http://www.ncbi.nlm.nih.gov/pubmed/17364730

Fatt, I., 1978. Physiology of the eye: An introduction to the vegetative functions. Butterworths, London.

Freegard, T. J., jan 1997. The physical basis of transparency of the normal cornea. Eye 11 (Pt 4), 465–471.
URL http://www.ncbi.nlm.nih.gov/pubmed/9425408

Glass, D. H., Roberts, C. J., Litsky, A. S., Weber, P. a., sep 2008. A viscoelastic biomechanical model of the cornea describing the eff ect of viscosity and elasticity on hysteresis. Investigative ophthalmology & visual science 49 (9), 3919–26.
URL http://iovs.arvojournals.org/article.aspx?articleid=2164254http://www.ncbi.nlm.nih

Grytz, R., Meschke, G., oct 2009. Constitutive modeling of crimped collagen fibrils in soft tissues. Journal of the mechanical behavior of biomedical materials 2 (5), 522– 533.
URL http://www.ncbi.nlm.nih.gov/pubmed/19627859

Grytz, R., Meschke, G., apr 2010. A computational remodeling approach to predict the physiological architecture of the collagen fibril network in corneo-scleral shells. Biomechanics and modeling in mechanobiology 9 (2), 225–235.
URL http://www.ncbi.nlm.nih.gov/pubmed/19802726

Holzapfel, G. A., 2000. Nonlinear solid mechanics: a continuum approach for engineer-ing, 1st Edition. Wiley.

Holzapfel, G. A., Gasser, T. C., 2001. A viscoelastic model for fiber-reinforced composites at finite strains: Continuum basis, computational aspects and applications. Computer methods in applied mechanics and . . . 190.
URL http://www.sciencedirect.com/science/article/pii/S0045782500003236

Holzapfel, G. A., Gasser, T. C., Ogden, R. A. Y. W., 2000. A new constitutive framework for arterial wall mechanics and a comparative study of material models. Journal of Elasticity (61), 1–48.

Jue, B., Maurice, D. M., Ophthalmology, D., Stanford, M., jan 1991. The mechanical properties of the rabbit and human cornea. Journal of Biomechanics 24 (9), 869–872. URL http://www.ncbi.nlm.nih.gov/pubmed/1752871

Kling, S., Bekesi, N., Dorronsoro, C., Pascual, D., Marcos, S., jan 2014. Corneal viscoelastic properties from finite-element analysis of in vivo air-puff deformation. PloS one 9 (8), e104904.
URL http://journals.plos.org/plosone/article?id=10.1371/journal.pone.0104904

Komai, Y., Ushiki, T., jul 1991. The three-dimensional organization of collagen fibrils in the human cornea and sclera. Investigative Ophthalmology & Visual Science 32 (8), 2244–58.
URL http://www.ncbi.nlm.nih.gov/pubmed/2071337

Markert, B., Ehlers, W., Karajan, N., dec 2005. A general polyconvex strain-energy function for fiber-reinforced materials. PAMM 5 (1), 245–246.
URL http://doi.wiley.com/10.1002/pamm.200510099

Meek, K. M., Boote, C., mar 2004. The organization of collagen in the corneal stroma. Experimental Eye Research 78 (3), 503–512.
URL http://linkinghub.elsevier.com/retrieve/pii/S0014483503002379

Newton, R. H., Meek, K. M., jun 1998. Circumcorneal annulus of collagen fibrils in the human limbus. Investigative Ophthalmology & Visual Science 39 (7), 1125–34. URL http://www.ncbi.nlm.nih.gov/pubmed/9620071

Nguyen, T. D., Boyce, B. L., jun 2011. An inverse finite element method for determining the anisotropic properties of the cornea. Biomechanics and modeling in mechanobi-ology 10 (3), 323–337.
URL http://www.ncbi.nlm.nih.gov/pubmed/20602142

Nguyen, T. D., Jones, R. E., Boyce, B. L., aug 2008. A nonlinear anisotropic viscoelas-tic model for the tensile behavior of the corneal stroma. Journal of biomechanical engineering 130 (4), 041020.
URL http://biomechanical.asmedigitalcollection.asme.org/article.aspx?articleid=1421573

Oyster, C., 1999. The human eye: structure and function. Sinauer Associates Inc., Sunderland.

Pandolfi, A., Holzapfel, G. a., dec 2008. Three-dimensional modeling and computa-tional analysis of the human cornea considering distributed collagen fibril orienta-tions. Journal of biomechanical engineering 130 (6), 61006.
URL http://www.ncbi.nlm.nih.gov/pubmed/19045535

Pandolfi, A., Manganiello, F., nov 2006. A model for the human cornea: constitutive formulation and numerical analysis. Biomechanics and modeling in mechanobiology 5 (4), 237–46.
URL http://www.ncbi.nlm.nih.gov/pubmed/16444515

Perez, B. C., Morris, H. J., Hart, R. T., Liu, J., dec 2013. Finite element modeling of the viscoelastic responses of the eye during microvolumetric changes. Journal of biomedical science and engineering 6 (12A), 29–37.
URL http://www.scirp.org/journal/PaperInformation.aspx?PaperID=40830{&}{#}abstract

Petsche, S. J., Pinsky, P. M., jan 2013. The role of 3-D collagen organization in stromal elasticity: a model based on X-ray diff raction data and second harmonic-generated images. Biomechanics and modeling in mechanobiology (1938).
URL http://www.ncbi.nlm.nih.gov/pubmed/23288406

Pinsky, P. M., van der Heide, D., Chernyak, D., jan 2005. Computational modeling of mechanical anisotropy in the cornea and sclera. Journal of Cataract & Refractive Surgery 31 (1), 136–45.
URL http://www.ncbi.nlm.nih.gov/pubmed/15721706

Studer, H., Larrea, X., Riedwyl, H., B¨uchler, P., mar 2010. Biomechanical model of human cornea based on stromal microstructure. Journal of biomechanics 43 (5), 836– 42.
URL http://www.ncbi.nlm.nih.gov/pubmed/20006338

Su, P., Yang, Y., Xiao, J., Song, Y., 2015. Corneal hyper-viscoelastic model: derivations, experiments, and simulations. Acta of Bioengineering and Biomechanics 17 (2), 73–84.

Whitford, C., Studer, H., Boote, C., Meek, K. M., Elsheikh, A., feb 2015. Biomechanical model of the human cornea: Considering shear stiffness and regional variation of collagen anisotropy and density. Journal of the Mechanical Behavior of Biomedical Materials 42 (September 2015), 76–87.
URL http://linkinghub.elsevier.com/retrieve/pii/S1751616114003476http://www.scienced

Page 3: [1] Deleted	Elsheikh	23/09/2016 08:35:00

3

Page 4: [2] Deleted	Elsheikh	23/09/2016 08:35:00

responses. Where (1) represents dilation, (2) describes the isotropic matrix distortion response in both tension and compression stiff ness, (3) activated only under tensile strain, represents the anisotropic and regional variation of collagen fibrils.